

Kinetic rates and free-energy-relationships for water dissociation on transition and noble metal dimers

Constantinos D. Zeinalipour-Yazdi*¹ and Rutger A. van Santen²

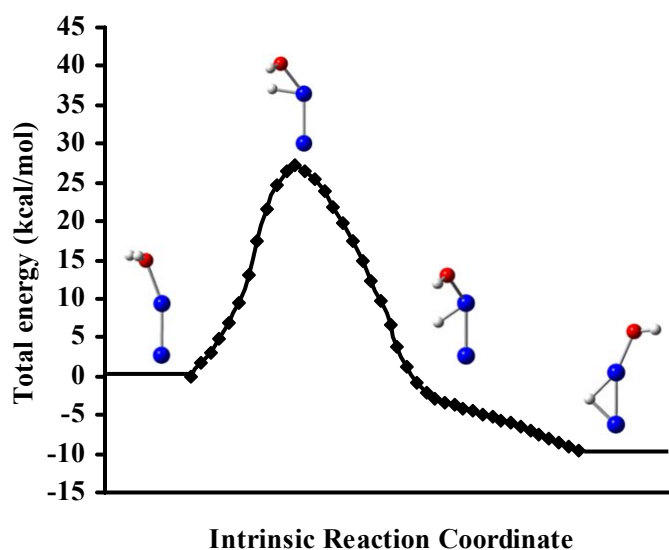
¹Department of Chemistry, University of Cyprus, CY 1678, Nicosia, Cyprus

²Schuit Institute of Catalysis, Eindhoven University of Technology, P.O.Box 513, Eindhoven, Netherlands

* Corresponding Author. E-mail address: zeinalip@ucy.ac.cy, (C.D. Zeinalipour)

TITLE RUNNING HEAD: Kinetic rates and free-energy-relationships for water dissociation on transition and noble metal dimers

Table of Contents (TOC) graphic



Abstract

A systematic study of the adsorption and dissociation of water on transition and noble metal dimers (Fe_2 , Ru_2 , Os_2 , Co_2 , Rh_2 , Ir_2 , Ni_2 , Pd_2 , Pt_2 , Cu_2 , Ag_2 , Au_2) is

presented. Spin unrestricted density functional theory simulations indicate that the dissociation (lysis) of water on these clusters may be thermally driven even in the absence of other electrocatalytically and photocatalytically driven processes. Two reaction pathways are found with turn-over-frequencies for water dissociation given by the following series $\text{Co}_2 > \text{Ir}_2 > \text{Fe}_2 > \text{Rh}_2 > \text{Ni}_2 > \text{Pt}_2 > \text{Ru}_2 > \text{Os}_2 > \text{Cu}_2 > \text{Au}_2 > \text{Pd}_2 > \text{Ag}_2$ at standard ambient temperature and pressure. Linear-free energy relationships are presented, that can predict the dissociation barrier of water on transition and noble metals as a function of free energy change for dissociation.

I. Introduction

Finding materials that have enhanced activity towards the dissociation (lysis) of water is of importance for the production of molecular hydrogen (H_2) from water^{1,2} and for the use of water as a hydration agent^{3,4}. During the 60's, after the first energy crisis, efforts had been made to find catalysts that can produce molecular hydrogen from water. Water is abundant in nature and the fact that the oxidation of H_2 yields water means that it can be infinitely recycled with no major waste products, thus claimed to be the most environmentally friendly fuel currently known. It has been previously suggested that transition metal catalysts that have a low barrier for the dehydrogenation of water could be utilized for the production of molecular hydrogen⁵⁻⁷. Laser ionization and time-of-flight mass spectroscopy experiments of neutral Fe_{7-17} clusters⁸, showed evidence of H_2 evolution upon the reaction with gas-phase water, whereas neutral Pt_{7-30} clusters⁹ form water when exposed to H_2 and O_2 . However, as evident by the highly negative Gibbs free energy of formation of gas phase water ($\Delta_f G_{298\text{K}} = -54.63 \text{ kcal/mol}$)¹⁰, an

external energy source (e.g. heat, UV/Vis radiation, electricity) may be required to lead to the dissociation of H₂O, the evolution of H₂ and especially the desorption of O₂.

In this work, the simplest possible cluster of transition and noble metals, the dimer, is examined in order to gain further insight towards the understanding of metal reactivity towards the adsorption and dissociation of water. We hope that these model studies are of some relevance to larger nanoparticles under more realistic environments and that they will aid in the finding of transition-metal-cluster-based catalysts with high efficiency towards the thermocatalytic dissociation of water. Our interest in cluster-adsorbate chemistry stems from the fact that these clusters represent better highly uncoordinated sites on highly dispersed transition metal supported catalysts where Taylorian¹¹ rather than Langmuirian¹² driven reaction rates become more significant. For the first process the reaction rates are controlled by defects and highly uncoordinated sites that are sometimes present only in small numbers in extended defect-free surfaces,¹³ but significant in transition metal clusters and nanoparticles. In addition, transition metal dimers, such as Fe₂ or NiFe are found in the catalytic center of hydrogenases of green algae and cyanobacteria, used for hydrogen production or dissociation, and have been suggested for the use in bio-fuel cells or the industrial production of “bio-hydrogen”.¹⁴

There has been an increased number of quantum mechanical studies that explore the adsorption of water on small transition metal clusters¹⁵⁻²⁰ but only a limited number of studies that explore the dissociation of water^{21,22} or the interaction of the dissociation products (H, OH, O) with transition metals²³. The computational study of the adsorption and dissociation of water on transition metal surfaces has recently been brought back as an interesting research topic²⁴⁻²⁸ as well as the diffusion of water on metal surfaces^{29,30}.

The effect of co-adsorbed CO for water dissociation in a water bilayer and the effect of various bimetallic metal surfaces³¹ has also been explored.

The trends of water adsorption and dissociation on transition metal (TM) and noble metal (NM) dimers, M_2 (where $M = \text{Fe, Ru, Os, Co, Rh, Ir, Ni, Pd, Pt, Cu, Ag, Au}$) presented here, may be useful also as a qualitative guide to rationalize the dissociation kinetics of water on highly-dispersed transition metal supported catalysts at ambient temperature and pressure, in the absence of other photocatalytic and electrocatalytic phenomena.

The subsequent sections are organized in the following order. Initially we present a brief description of the computational methodologies used. Then, in Section A we locate the most stable spin multiplicity for each dimer and in Section B the optimized structures of adsorbed water, dissociated water and the transition states for water dissociation on the dimers. In Section C the trends of water adsorption/dissociation on all dimers are presented and in Section D expressions for the turn-over-frequency for water dissociation are derived and used to assess the activity trends for the dissociation of water on transition and noble metal dimers. Finally, in Section E linear-free-energy relationships are presented for the dissociation of water for the mechanistic pathways located in Section B.

II. Methods

Restricted and unrestricted Density Functional Theory (DFT) computations are employed, as implemented in Gaussian 03,³² with the use of Becke's three-parameter hybrid exchange functional³³ (XC) combined with the Lee-Yang-Parr non-local

correlation functional³⁴, abbreviated as B3LYP and UB3LYP, respectively. Initially an extended basis set saturation test was performed (see Table 1) using the Stevens/Basch/Krauss Effective Core Potential (ECP) triple-split basis, denoted as CEP-121G³⁵⁻³⁷ and the correlation consistent augmented valence triple zeta basis sets of the type aug-cc-pVXZ³⁸⁻⁴², where X = D, T, Q, to establish the quality of our computational setup. Linear dependencies of the basis functions were removed by using the spherical version (5d, 7f) of this basis set.

TABLE 1: Basis set tests for water adsorption on copper dimer using B3LYP. $\Delta E_{\text{non-BSSE}}$ is the adsorption energy not corrected for BSSE, ΔE_{BSSE} is the adsorption energy corrected for BSSE and ΔH is the enthalpy change for water adsorption at standard ambient temperature and pressure (SATP, P = 1bar, T = 298.15K). The total energies of water, the Cu dimer and water/Cu₂ energies for the various basis sets are given as supporting information (S-Table 1).

H ₂ O basis set	Cu basis set	$\Delta E_{\text{non-BSSE}}$ (kcal/mol)	ΔE_{BSSE} (kcal/mol)	ΔH (kcal/mol)
aug-cc-pVDZ	CEP-121G	-11.2	-10.3	-10.0
cc-pVTZ	CEP-121G	-13.5	-10.9	-12.3
aug-cc-pVTZ	CEP-121G	-11.7	-10.0	-10.5
cc-pVQZ	CEP-121G	-12.3	-11.2	-11.1
aug-cc-pVQZ	CEP-121G	-12.3	-10.5	-11.1
aug-cc-pVDZ	cc-pVDZ	-13.3	-10.7	-12.1
aug-cc-pVTZ	aug-cc-pVDZ	-11.8	-11.8	-10.5
aug-cc-pVTZ	cc-pVTZ	-11.7	-10.9	-10.5
aug-cc-pVTZ	aug-cc-pVTZ	-11.6	-11.4	-10.4
aug-cc-pVTZ	cc-pVQZ	-11.5	-11.2	-10.3

Basis Set Superposition Error (BSSE) corrections were performed using the counterpoise method of Boys and Bernardi⁴³. All computations were performed using the restricted or unrestricted B3LYP/CEP-121G(TM),aug-cc-pVTZ(O,H) method, unless otherwise noted, as a good compromise between computational accuracy and demand. This basis set choice yields water adsorption energies within 1 kcal/mol of the value obtained with the largest BSSE corrected basis set.

We adopted a computational strategy whereby all structures were fully optimized, to consider adsorption induced structural changes to the metal dimer and various starting configurations to ensure that all possible adsorbate/cluster configurations have been explored. Open shell computations were examined for spin contamination, which was found to be negligible. Local minima for the reaction intermediates and transition states (TS) have been confirmed by vibrational analysis, by the absence and presence of one imaginary vibrational frequency, respectively. Transition state structures were either located using the Synchronous Transit-Guided Quasi-Newton (STQN) method of Schlegel and co-workers^{44,45} or by scanning a particular bond length at a 0.05 Å resolution and relaxing the remaining atoms. The imaginary frequency of the located TS was examined to check that it corresponds to the desired reaction coordinate. Potential energy surface scans were obtained by a combined relaxed potential energy surface scan and the intrinsic reaction coordinate (IRC) method^{46,47} of the M-M-O angle and O-H bond, respectively.

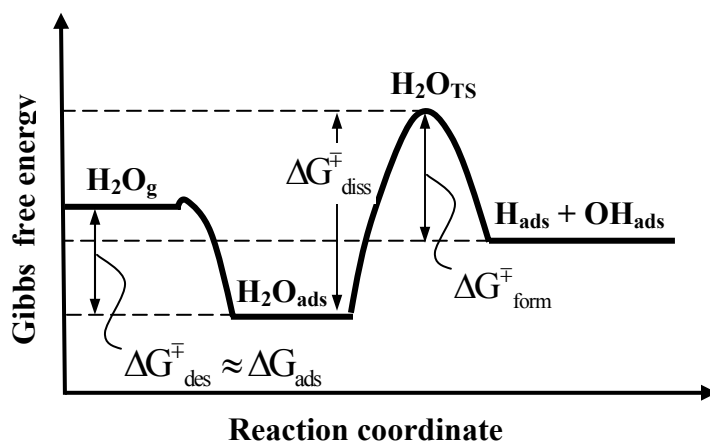


FIGURE 1: Simplified schematic of the potential energy curve for water dissociation on the various TM and NM dimers. Symbols are explained in the text.

The free energies barriers evaluated are presented in FIG. 1. The Gibbs free energy change for water adsorption (ΔG_{ads}) and the barriers for water dissociation ($\Delta G_{\text{diss}}^{\ddagger}$), formation ($\Delta G_{\text{form}}^{\ddagger}$) and desorption ($\Delta G_{\text{des}}^{\ddagger}$) were calculated using,

$$\Delta G_{\text{ads}} = G_{\text{M}_2\text{-H}_2\text{O}}^{\circ} - G_{\text{M}_2}^{\circ} - G_{\text{H}_2\text{O}}^{\circ} \quad (3)$$

$$\Delta G_{\text{diss}}^{\ddagger} = G_{\text{M}_2\text{-TS}}^{\circ} - G_{\text{M}_2\text{-H}_2\text{O}}^{\circ} \quad (4)$$

$$\Delta G_{\text{form}}^{\ddagger} = G_{\text{M}_2\text{-TS}}^{\circ} - G_{\text{M}_2\text{-OH-H}}^{\circ} \quad (5)$$

$$\Delta G_{\text{des}}^{\ddagger} = G_{\text{M}_2}^{\circ} + G_{\text{H}_2\text{O}}^{\circ} - G_{\text{M}_2\text{-H}_2\text{O}}^{\circ} \quad (6)$$

,where $G_{\text{M}_2\text{-H}_2\text{O}}^{\circ}$, $G_{\text{H}_2\text{O}}^{\circ}$, $G_{\text{M}_2\text{-TS}}^{\circ}$ and $G_{\text{M}_2\text{-OH-H}}^{\circ}$ are the Gibbs free energies of the adsorbed water/cluster complex, gas phase water, the cluster-water transition state complex and the dissociated water/cluster complex, respectively and $^{\circ}$ represents standard ambient temperature and pressure conditions (SATP, P = 1bar, T = 298.15K). Similar relationships were used for the total energy change (ΔE) and the enthalpy change (ΔH).

III. Results

A. Locating the most stable metal cluster

Initially the most stable spin multiplicity (M_s) for the TM and NM dimers was located through a careful series of calculations at different spin multiplicities (SM). The results for each group of transition metals are presented in FIG. 2. It can be clearly seen that the dimers that belong to the same group prefer the same spin multiplicities, for their most stable electronic configurations. Thus, metals with d^9 , d^8 , d^7 and d^6 electronic configurations of their valence electrons, had their most stable spin multiplicity equal to

1, 3, 5 and 7, respectively. The existence of unpaired electrons in these dimers cause the emergence of high magnetic properties as recently addressed^{48,49}. The largest variation of the relative total energy as a function of spin multiplicity is observed for the d^9 group of transition metals. For these metals a definite spin singlet state, is energetically preferred due to the important energy difference of 34.6 kcal/mol, compared to the triplet state. The energy difference becomes even more pronounced for higher spin multiplicity states, where energy differences as high as 346 kcal/mol were computed. Important variations of the relative energy among the dimers belonging to the same group are also seen for the d^8 , d^7 and d^6 metals. Thus, it is expected that in a real sample the dimers would almost entirely populate a particular spin multiplicity state for most of the metals examined with the exception of Co_2 and Ir_2 where the energy difference was 1.2 and 0.7 kcal/mol, respectively, when SMs of 5 and 7 were compared. These values were of the order of the thermal motion at room temperature ($RT = 0.6$ kcal/mol) thus, both states are expected in a real sample of these dimers. Nevertheless, in order to avoid spin transitions along the reaction pathway during the dissociation of water the water/dimer complex SM was kept fixed to that of the most stable dimer. This assumption was checked for the dimers that had close lying energetic states for different SM (e.g. Co_2 and Ir_2).

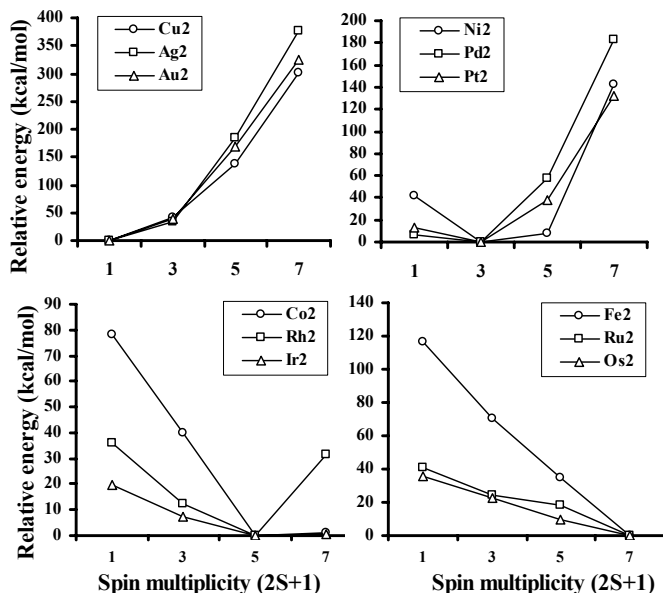


FIGURE 2: Relative total energies of mononuclear transition and noble metal dimers as a function of spin multiplicity ($2S+1$). S is the number of unpaired electrons in the metal dimer. The data points are tabulated in S-TABLE 2 in the supporting information.

B. Optimized cluster adsorbate structures

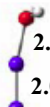
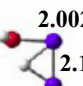
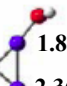
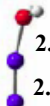
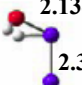
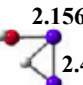
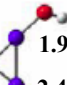
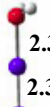
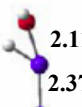
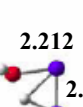
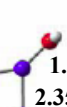
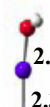
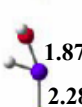
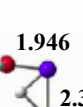
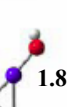
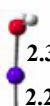
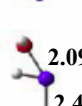
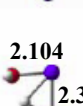
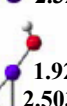
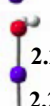
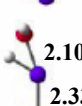
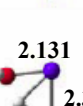
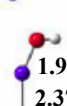
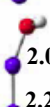
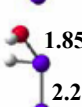
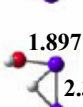
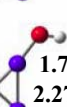
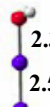
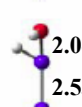
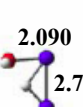
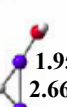
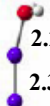
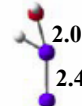
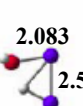
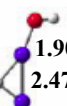
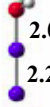
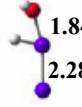
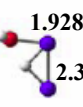
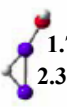
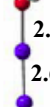
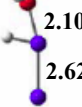
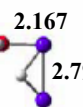

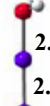
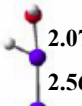
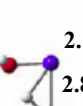
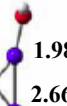
The configuration of adsorbed water (M_2-H_2O), the two possible transition states (M_2-TS1 , M_2-TS2) towards water dissociation and the dissociation products (M_2-OH-H) are presented in FIG. 3. Although the electronic structure among the various dimers is drastically different it was intriguing to observe a universality of the binding structures for the adsorbed, transition and dissociated state of water on these dimers. For all metals studied the atop binding mode for water was found to be the energetically preferred. This was checked by considering various initial configurations among which, either the water oxygen is bound to both metals or the water O-H is pointing perpendicularly towards the M-M bond. Interaction of the lone electron pair of water with the M-M bond (coordination of water in a bridged configuration) of the dimers was not observed in any case. In particular, the energetically preferred binding mode of water exhibited a weakly

hindered rotation around its molecular axis. Furthermore, the molecular axis of water had a tilt angle, with respect to the molecular axis of the dimer, by about 60° . This clearly indicates the interaction of the lone electron $1b_1$ of water with the unsaturated electron density at the metal site. The adsorption structure identified here resembles the one predicted by DFT for water monomer adsorption on TM surfaces.²⁶ For all clusters the metal-oxygen bond length (R_{MO}) decreases as a function of the O-H bond length during the progress of the reaction towards the dissociated form of water, having the following order



A similar trend for the M-O bond length is found for TS2. This suggests that electron density from the M-O bond is pushed into the region of the O-H bond favoring the elongation of the O-H bond and its scission after a critical O-H separation of about 1.5 Å. This is in agreement with the common notion that the transition metal atom activates the O-H bond and lowers the activation barrier for the dissociation, compared to the gas phase dissociation barrier, which is drastically higher (≈ 160 kcal/mol). In particular, during the dissociation the metal-oxygen bond decreases by 0.3 – 0.5 Å, while at the same time the O-H increases by 0.5 – 1.0 Å to reach the TS point.

FIGURE 3: Optimized molecular geometries of various $M_2\text{-H}_2\text{O}$ clusters, where $M = \text{Fe, Ru, Os, Co, Rh, Ir, Ni, Pd, Pt, Cu, Ag, Au}$, showing selected bond lengths. The various metals, carbon and oxygen shown in black, white and dark grey, respectively. The optimized lengths of the M-M and M-O bonds are reported in Angstroms.

M	$M_2\text{-H}_2\text{O}$	$M_2\text{-TS1}$	$M_2\text{-TS2}$	$M_2\text{-OH-H}$
Fe	 2.165 2.032	n/a	 2.002 2.138	 1.806 2.369
Ru	 2.486 2.357	 2.134 2.391	 2.156 2.425	 1.966 2.447
Os	 2.361 2.301	 2.112 2.379	 2.212 2.332	 1.935 2.357
Co	 2.105 2.317	 1.878 2.288	 1.946 2.345	 1.801 2.320
Rh	 2.371 2.261	 2.091 2.411	 2.104 2.397	 1.922 2.503
Ir	 2.271 2.288	 2.101 2.335	 2.131 2.354	 1.927 2.377
Ni	 2.061 2.296	 1.854 2.283	 1.897 2.375	 1.761 2.270
Pd	 2.399 2.537	 2.041 2.538	 2.090 2.703	 1.956 2.662
Pt	 2.271 2.386	 2.063 2.433	 2.083 2.504	 1.907 2.473
Cu	 2.082 2.275	 1.844 2.288	 1.928 2.368	 1.789 2.353
Ag	 2.474 2.610	 2.100 2.621	 2.167 2.795	 2.028 2.721
Au	 2.329 2.558	 2.072 2.562	 2.102 2.848	 1.984 2.664

Concerning the reaction mechanism for water dissociation on TM and NM dimers, two major reaction pathways were located. In the first pathway (*pathway 1*, FIG. 4a) the O-H bond length increases in length, to a critical value of about 1.5 Å, which results in the migration of hydrogen to the same metal atom where water was initially adsorbed. Such a transition state can be obtained by one of the two stretching modes of water (ν_s, ν_a), which then lead to a complete dissociation of the O-H bond activated by the presence of the metal atom. The hydrogen then can easily diffuse through two rather small diffusion barriers, the first to overcome repulsive interactions with M-M unbound orbitals and the second to bound M-M orbitals, to finally obtain an energetically favored bridged configuration. This process is observed for all transition metals except Ir₂ and Os₂, where a linearly adsorbed final state for hydrogen was found.

The second water dissociation pathway (*pathway 2*, FIG. 4b) is one where the initial angle ($\sim 180^\circ$) between the M-M and M-O bond decreases to a value of ($\sim 80^\circ$) where the O-H bond becomes almost parallel to the M-M bond, which then dissociates to form a bridged hydrogen and a linearly adsorbed hydroxyl group. It is noted that both dissociation pathways can occur on extended (111) surfaces of TM and NM, as previously pointed out.^{24,50} Importantly it is noted that due to differences in the relative dissociation barriers of water dissociation *pathway 1* and *2*, not all TMs will follow the same dissociation pathway. In particular, for Os₂, Co₂, Ni₂ and Pt₂ can essentially follow both dissociation pathways, Fe₂, Ru₂, Rh₂, Pd₂, Cu₂ and Ag₂ follow only *pathway 2* and Ir₂ and Au₂ only *pathway 1*. It is suggested that the barriers for both pathways are explored in future studies of the dissociation of water on transition and noble metals.

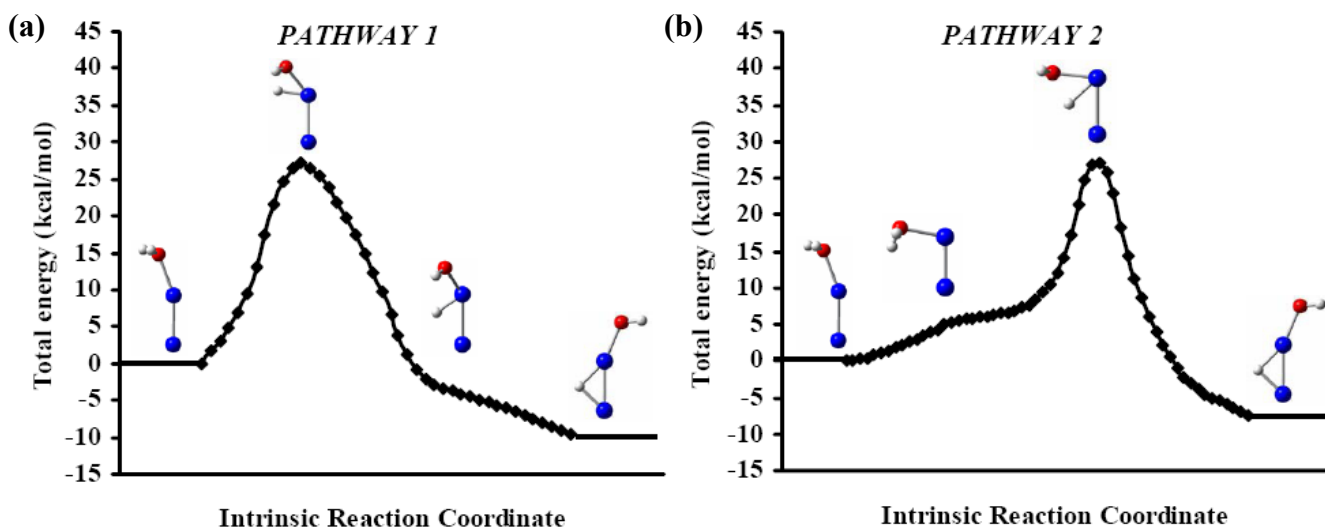


FIGURE 4: Potential energy curves for (a) *pathway 1* and (b) *pathway 2* of the dissociation of water on Ni₂.

C. Trends of water adsorption energies and dissociation barriers

The trends of energy (ΔE), enthalpy (ΔH) and Gibbs free energy (ΔG) change upon water adsorption and dissociation on transition and noble metal dimers are presented in FIG. 5a and 5b, respectively. Most of these transition metals (Pt, Os, Fe, Rh, Cu, Au, Ru) adsorb water weakly (2-5 kcal/mol), Ir and Ni adsorb water moderately (12-17 kcal/mol), Co yielded a surprisingly large adsorption energy of 43.7 kcal/mol, whereas Ag and Pd were found not to adsorb water at all. In order to test the validity of the surprisingly high adsorption energy of water on Cobalt a series of additional computations at the other SM were performed yielding adsorption energies of 5.61, -34.6 and -13.7 kcal/mol for SM of 1, 3 and 7, respectively. However the relative energy of Co₂-H₂O complex at a SM of 5 was the most stable by 16 kcal/mol compared to the complex with SM 7, that was the closest in energy among the various SMs considered. It is interesting to note that generally for extended surfaces experimental evidence from

temperature-programmed desorption of water suggest that in the T range between 200-350K water does not generally adsorb, whereas polycrystalline surfaces exhibit water adsorption.^{7,51} This is in agreement with the result found here that show that all transition and noble metal dimers, except Ag₂ and Pd₂, adsorb water.

The trends for the free energy barrier for water dissociation on the transition metal dimers studied are given in FIG. 5b. As expected, the dissociation barrier of transition metal activated water dissociation studied here is lower than that of gas phase water (≈ 160.6 kcal/mol) dissociation. It is observed that only for the case of Co₂ and Ir₂ the free energy barrier for water dissociation is lower than the desorption energy barrier ($-\Delta G_{\text{ads}}$), thus, it is expected that during the thermolytically driven dissociation of water on transition and noble metal dimers, water will prefer to dissociate rather than desorb. The catalysts *TOFs* derived in the following section will clearly demonstrate this effect. Although usually the catalytic activity of extended surfaces will be quite different from the results obtained on clusters, we observe that the trends obtained from the water/cluster models examined here compare well with the trends obtained on extended surfaces. In particular, Wang *et al.*⁵⁰ found that the activation barrier for water dissociation on (111) surfaces, follows the trend Au<Ag<Cu<Pd<Rh<Ru<Ni, whereas we find a quite similar trend, Au<Ag<Cu<Pd \approx Ni<Ru<Rh when considering the TS2 activation barrier, which is the relevant transition state used in that study.to the surface dissociation state.

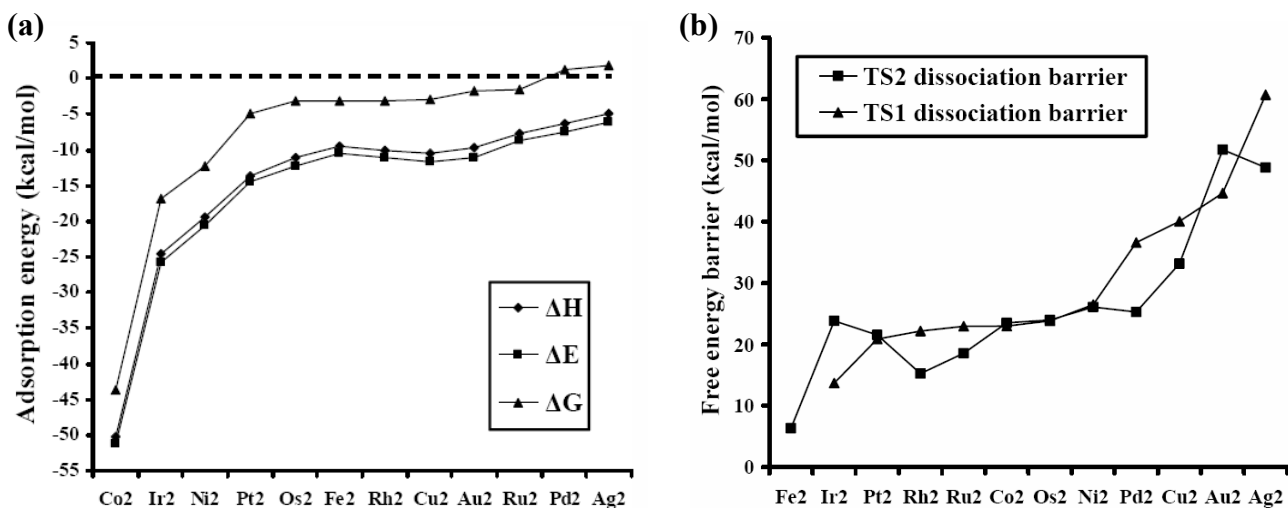


FIGURE 5: Trends of energy (ΔE), enthalpy (ΔH) and Gibbs free energy (ΔG) change for (a) water adsorption and (b) water dissociation barriers on group VIIIB and IB transition metal dimers. The data points are tabulated in S-TABLE 3, given as supporting information.

D. Water dissociation activity trends

The purpose of this section is to derive reactivity series for the dissociation of water on transition and noble metal dimers. This series should also qualitatively hold for the active sites of Taylorian¹¹ catalysts, but one should note that for larger particles these sites may just be a small fraction of the particles' exposed surface. The reaction steps for water dissociation are given by the following mechanistic steps,



Thus, one can write the rate for water adsorption and water dissociation as,

$$-\frac{d[H_2O_g]}{dt} = k_{ads} [H_2O_g] - k_{des} [H_2O_{ads}] \quad (7)$$

$$-\frac{d[H_2O_{ads}]}{dt} = k_{diss} [H_2O_{ads}] - k_{form} [OH_{ads}][H_{ads}] \quad (8)$$

, respectively where k_i is the rate constant of i and $[i]$ the corresponding concentration of i . In order to get an estimate of the reactant and products surface concentrations first we assume that the water dissociation mechanism is at equilibrium. Since at equilibrium Eqns 7-8 equal to zero one can write that,

$$\frac{k_{ads}}{k_{des}} = \frac{[H_2O_{ads}]}{[H_2O_g]} \quad (9)$$

$$\frac{k_{diss}}{k_{form}} = \frac{[OH_{ads}][H_{ads}]}{[H_2O_{ads}]} \quad (10)$$

Using the definition of the reaction equilibrium constant one obtains,

$$K_{eq} = \frac{[OH_{ads}][H_{ads}]}{[H_2O_g]} = \frac{k_{diss}k_{ads}}{k_{form}k_{des}} \quad (11)$$

Using the definition for the rate constant from transition state theory⁵²,

$$k_i = \frac{k_B T}{h} \exp\left(\frac{-\Delta G_i^\ddagger}{RT}\right) \quad (12)$$

where k_B , T , h , ΔG_i^\ddagger , R are the Boltzmann constant, the temperature, Planck constant, the Gibbs free energy barrier of i and the gas constant, respectively. Taking into account that the barrier for water adsorption is essentially zero ($\Delta G_{ads}^\ddagger \cong 0$) for all metals studied, one can write the equilibrium constant as a function of first principles derived free energy barriers,

$$K_{eq} = \frac{\exp\left(\frac{-\Delta G_{diss}^\ddagger}{RT}\right)}{\exp\left(\frac{-\Delta G_{form}^\ddagger}{RT}\right) \exp\left(\frac{-\Delta G_{des}^\ddagger}{RT}\right)} \quad (13)$$

If we assume that a regular Langmuir isotherm describes the adsorption of water to the cluster and that each metal atom in the cluster in cooperation with an adjacent M-M bond can dissociate a single water molecule then we can write that,

$$\theta_{H_2O} = \frac{K(p_{H_2O}/p^\ominus)}{1 + K(p_{H_2O}/p^\ominus)} \quad (14)$$

, where

$$K = \frac{k_{ads}}{k_{des}} = \exp\left(\frac{-\Delta G_{des}^\ddagger}{RT}\right) \quad (15)$$

and p_{H_2O} is the partial pressure of water in the feedstream ($p^\ominus = 1$ bar). Substitution of Eqn. 11 into Eqn. 8 and replacing concentrations with the corresponding surface coverages and partial pressures, yields,

$$-\frac{d[H_2O_{ads}]}{dt} = k_{diss}\theta_{H_2O} - k_{form}K_{eq}\frac{p_{H_2O}}{p^\ominus} \quad (16)$$

So the catalysts turn-over-frequency (*TOF*) for water dissociation is given by combination of Eqns 11-16, which yields,

$$TOF = \frac{p_{H_2O}k_B T}{p^\ominus h} \left[\frac{\exp\left(-\Delta G_{diss}^\ddagger/RT\right)\exp\left(-\Delta G_{des}^\ddagger/RT\right)}{1 + \exp\left(-\Delta G_{des}^\ddagger/RT\right)\frac{p_{H_2O}}{p^\ominus}} - \frac{\exp\left(-\Delta G_{diss}^\ddagger/RT\right)}{\exp\left(-\Delta G_{des}^\ddagger/RT\right)} \right] \quad (17)$$

Finally using Eqn. 17 and the DFT derived thermodynamic activation barriers ($\Delta G_{diss}^\ddagger, \Delta G_{des}^\ddagger$) and equilibrium constants (K_{eq}) shown in TABLE 2 we evaluate the qualitative trends of *TOFs* among the various TM clusters. These results are presented in in FIG. 6. It is intriguing to observe that all TM dimers examined with the exception of Fe₂, Co₂ and Ir₂ will desorb water, rather than dissociate it at SATP. A surprisingly high activity was observed for Co₂, followed by Ir₂ (12 orders of magnitude lower *TOF*) and

Fe₂. On these transition metal dimers it is expected that water dissociation is kinetically favored even at room temperature and atmospheric pressure conditions. For Ag₂ and Pd₂ water dissociation is hindered by the positive free energy change (ΔG_{ads}) upon water adsorption, whereas for the remaining TMs the activity is low due to the lower activation barrier for water desorption compared to water dissociation barrier.

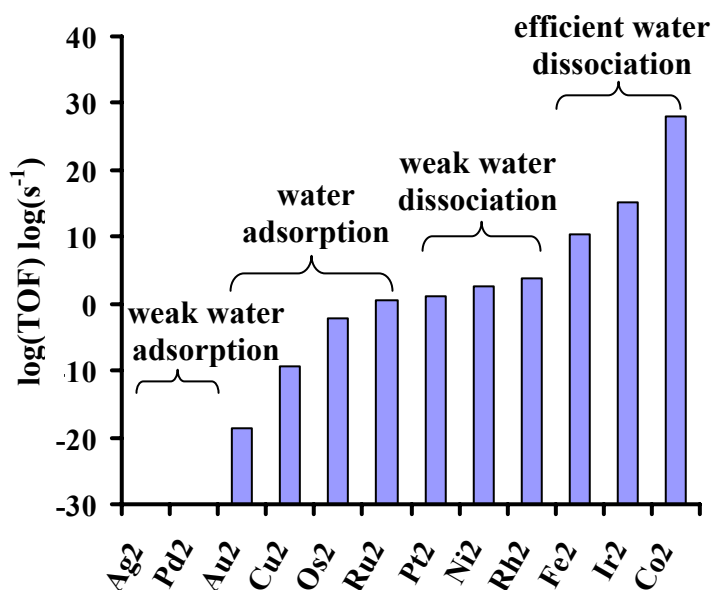


FIGURE 6: Bar diagram of *TOF* logarithm of the lowest energetic pathway for water dissociation on transition and noble metal dimers at SATP (298.15K, 1bar). The values of Pd₂ and Ag₂ have been omitted since their *TOFs* were negative due to their positive free energies of adsorption.

TABLE 2: Tabulated values for spin multiplicity, free energy barrier for water dissociation ($\Delta G^\ddagger_{\text{diss}}$), formation ($\Delta G^\ddagger_{\text{form}}$) and desorption ($\Delta G^\ddagger_{\text{des}}$) the thermodynamic equilibrium constant (K_{eq}) and the catalyst turn-over-frequency (TOF). Negative *TOFs* indicate no adsorption of water.

M_2	spin mult.	$\Delta G^\ddagger_{\text{des}}$ (kcal/mol)	$\Delta G^\ddagger_{\text{dissTS1}}$ (kcal/mol)	$\Delta G^\ddagger_{\text{dissTS2}}$ (kcal/mol)	$\Delta G^\ddagger_{\text{formTS1}}$ (kcal/mol)	$\Delta G^\ddagger_{\text{formTS2}}$ (kcal/mol)	K_{eq}	TOF (Hz)
Fe₂	7	3.2	-	6.3	-	53.6	1.03×10^{37}	3.20×10^{10}
Ru₂	7	1.6	22.9	18.6	35.1	30.7	1.28×10^1	2.39×10^0
Os₂	7	3.2	23.8	24.0	41.6	41.8	2.54×10^{15}	4.86×10^{-3}
Co₂	5	43.7	23.0	23.5	36.2	36.8	5.20×10^{41}	9.22×10^{27}
Rh₂	5	3.0	22.2	15.2	36.2	29.3	3.25×10^{12}	7.22×10^3
Ir₂	5	16.9	13.7	23.8	30.2	40.4	2.98×10^{24}	1.32×10^{15}
Ni₂	3	12.3	26.5	26.1	36.5	36.1	2.48×10^{16}	5.06×10^2
Pd₂	3	-1.2	36.6	25.3	30.0	18.7	1.80×10^{-6}	-1.35×10^{-6}
Pt₂	3	4.9	20.9	21.5	28.9	29.5	3.01×10^9	1.30×10^1
Cu₂	1	2.9	40.1	33.2	38.2	31.3	5.06×10^0	3.78×10^{-10}
Ag₂	1	-1.9	60.7	48.9	37.7	25.9	5.83×10^{-19}	-8.69×10^{-24}
Au₂	1	1.7	44.7	51.8	25.2	32.2	9.04×10^{-14}	2.02×10^{-19}

Although our model systems may not directly resemble the structure of evaporated films, we notice that the calculated *TOFs* correlate well with experimental evidence from Temperature Programmed Desorption Spectroscopy (TPDS), after water adsorption on evaporated Fe, Co, and Ni films⁵³. In particular, among the three, Co exhibited the most significant H₂ evolution starting at 280K with no concurrent water desorption. A similar behavior is observed for Fe, only at higher desorption temperatures (300K), whereas for Ni both water and hydrogen evolution are observed suggesting that both adsorbed water and dissociated water species are present, all in agreement with the *TOFs* presented in FIG 6.

It is interesting to note that supported Co catalyst are the most effective catalysts for the Fisher-Tropsch (F-T) reaction⁵⁴ used for hydrocarbon synthesis, followed in activity by Fe-supported catalysts, whereas nickel is also active. Our results show that all three transition metals have the ability to dissociate water efficiently, thus generating atomic hydrogen efficiently, which then can be utilized in hydrogenation reactions of adsorbed CO and other unsaturated carbohydrate species. Additionally, metals that are commonly used in metal-supported Water-Gas Shift (WGS) catalysts⁵⁵, such as Cu and Au exhibit non-dissociative water adsorption capability. So it is evident that the *TOF* trends presented here can aid to the rationalization of catalytic activity in very important industrial reactions (e.g. WGS, F-T).

E. Linear-free-energy relationships for the dissociation of water on transition metals

Linear-free-energy (LFE) relationships that correlate the free energy barrier ($\Delta G^\ddagger_{\text{diss}}$) for a particular reaction step to the free energy difference of the intermediates (ΔG_{diss}) involved in the step have been used for a long time in organic chemistry. Such relationships that were initially empirical are referred to as Brønsted-Evans-Polanyi (BEP) relationships.^{56,57} They are usually of the general form,

$$\Delta G^\ddagger_{\text{diss}} = \alpha \cdot \Delta G_{\text{diss}} + c \quad (18)$$

,where α and c are parameters that are empirically obtained. Recently, similar relationships have been derived on the basis of first principle computations, for dissociation and association reactions occurring in heterogeneously catalyzed reactions.⁵⁸⁻
⁶⁰ These relationships are particularly useful when estimation of reaction barriers⁶¹ is desirable or when catalytic activity trends⁶⁰ are to be rationalized. For the dissociation of

water two previous studies report the coefficients α and c with rather inconsistent results. In a seminal study⁶² that explores LFE relationships over various dehydrogenation reactions (e.g. O-H, C-H, N-H) on the (111) surface of transition and noble metals the following relationship was derived,

$$E_{\alpha}^{\text{diss}} = (0.92 \pm 0.05) \cdot \Delta H + (20 \pm 1) \quad (19)$$

It is noted that in this study the transition state for water dissociation was bound to the same atom, which resembles *pathway 1* of this study, whereas in another study⁵⁰ where the relationship,

$$E_{\alpha}^{\text{diss}} = (0.67 \pm 0.05) \cdot \Delta H + (26 \pm 1) \quad (20)$$

was found, the transition state is bound to two metal atoms, which resembles *pathway 2*.

In FIG. 7 the LFE graphs of *pathway 1* and *2* are presented that yielded the relationships,

$$\Delta G_{\text{diss,TS1}}^{\ddagger} = (0.9 \pm 0.1) \cdot \Delta G_{\text{diss}} + (34 \pm 2) \quad R = 0.94 \quad (21)$$

$$\Delta G_{\text{diss,TS2}}^{\ddagger} = (0.6 \pm 0.1) \cdot \Delta G_{\text{diss}} + (31 \pm 2) \quad R = 0.90 \quad (22)$$

, respectively. It is clear that the α coefficient obtained by the two previous studies are within the statistical error at 0.98 confidence bounds of the values obtained here. Thus, the results obtained remove the discrepancy between the previously reported LFE relationships, by assigning each to a different pathway for water dissociation. In contrast, a weaker agreement was found for the b coefficient suggesting that the finite size of the cluster employed, affects the value of only that coefficient. Furthermore, our results suggest that computationally inexpensive metal dimers can be readily utilized to obtain the α coefficient in LFE relationships for heterogeneously catalyzed reactions occurring on even larger particles.

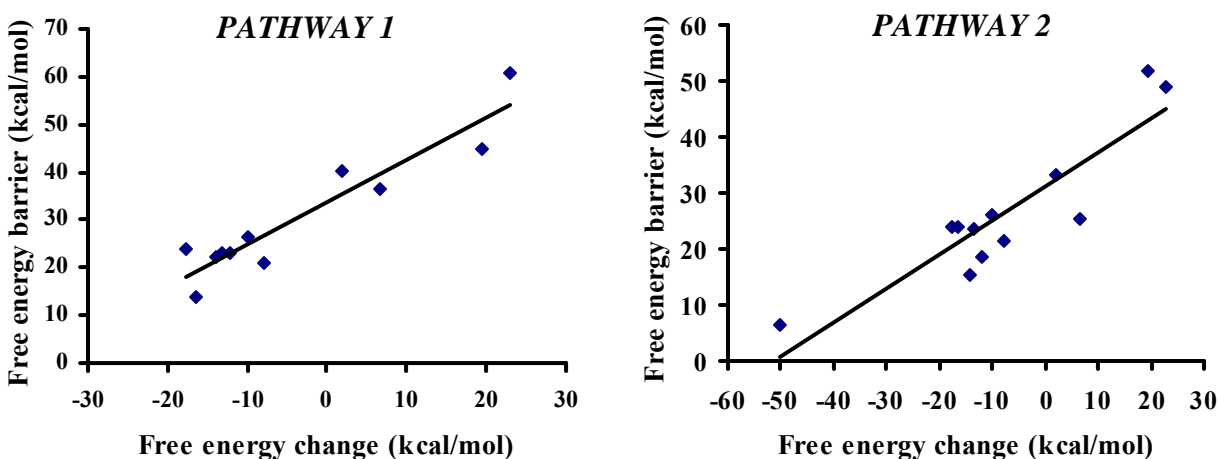


FIGURE 7: Linear-free-energy plots of (a) *pathway 1* and (b) *pathway 2* for the dissociation of water on transition and noble metal dimers. Data points are calculated based on the values presented in TABLE 2.

IV. Summary

In conclusion, the systematic study of water adsorption and dissociation on group VIIIIB and IB transition metal dimers (Fe_2 , Ru_2 , Os_2 , Co_2 , Rh_2 , Ir_2 , Ni_2 , Pd_2 , Pt_2 , Cu_2 , Ag_2 , Au_2) presented in this work shows that the dissociation (lysis) of water on these clusters may be thermally driven even in the absence of other electrocatalytically and photocatalytically driven processes. Linear-free energy relationships are presented, that can predict the dissociation barrier of water on transition and noble metals as a function of free energy change for dissociation. It is found that at standard ambient temperature and pressure the turn-over-frequency for water dissociation is given by the following series $\text{Co}_2 > \text{Ir}_2 > \text{Fe}_2 > \text{Rh}_2 > \text{Ni}_2 > \text{Pt}_2 > \text{Ru}_2 > \text{Os}_2 > \text{Cu}_2 > \text{Au}_2 > \text{Pd}_2 > \text{Ag}_2$. Cobalt, iridium and iron dimers performed particularly well and thus should be further considered as efficient catalysts that promote the dissociation of water in homogenous and

heterogeneous catalytic systems. The qualitative trends are expected to be valid and useful to experimentalists that need to choose among transition metals that adsorb water strongly and dissociate it efficiently. The study shows again the potential of using transition metal nanoclusters in heterogeneously or homogeneously reactions that catalyze the dissociation of water.

Acknowledgments

Fruitful discussions with Dr. Angelos Michaelides and the Thomas Young Research Fellowship (for C.D.Z.) from London Centre for Nanotechnology are warmly acknowledged.

Supporting Information Available

Total Gibbs free energies of the various water/metal clusters are given as supporting information (S-Table 4). This information is available free of charge via the internet at <http://pubs.acs.org>.

References:

- (1) Harriman, A. *Platinum Metals Rev.* **1983**, *27*, 102-107.
- (2) Samorjai, G. A.; Hendewerk, M.; Turner, J. E. *Cat. Rev.-Sci. Eng.* **1984**, *26*, 683.
- (3) Grotjahn, D. B.; Kragulj, E. J.; Zeinalipour-Yazdi, C. D.; Miranda-Soto, V.; Lev, D. A.; Cooksy, A. L. *J. Am. Chem. Soc.* **2008**, *130*, 10860-10861.
- (4) Grotjahn, D. B. *Dalton Trans.* **2008**, *46*, 6497-6508.
- (5) Heras, J. M.; Albano, E. V. *Appl. Surf. Sci.* **1983**, *17*, 207-219.
- (6) Heras, J. M.; Albano, E. V. *Appl. Surf. Sci.* **1983**, *17*, 220-230.
- (7) Heras, J. M.; Viscido, L. *Catal. Rev.* **1988**, *30*, 281-338.
- (8) Weiller, B. H.; Bechthold, P. S.; Parks, E. K.; Pobo, L. G.; Riley, S. J. *J. Chem. Phys.* **1989**, *91*, 4714-4726.
- (9) Andersson, M.; Rosén, A. *J. Chem. Phys.* **2002**, *117*, 7051-7054.

- (10) Wagman, D. D.; Evans, W. H.; Parker, V. B.; Schumm, R. H.; Halow, I.; Bailey, S. M.; Chumey, K. L.; Nuttall, R. L. *The NBS Tables of Chemical Thermodynamic Properties*, 1982.
- (11) Taylor, H. S. *Proc. Roy. Soc. A* **1925**, *105*, 9.
- (12) Langmuir, I. *Trans. Farad. Soc.* **1921**, *17*, 62.
- (13) van Santen, R. A.; Neurock, M. *Molecular Heterogeneous Catalysis: A conceptual and computational approach*; Wiley-VCH, 2006.
- (14) Fontecilla-Camps, J. C.; Volbeda, A.; Cavazza, C.; Nicolet, Y. *Chem. Rev.* **2007**, *107*, 4273-4303.
- (15) Anderson, A. B. *Surf. Sci.* **1981**, *105*, 159-176.
- (16) Holloway, S.; Bennemann, K. H. *Suf. Sci.* **1980**, *101*, 327-333.
- (17) Rosén, J. P. A. *Int. J. Quant. Chem.* **1983**, *23*, 1231-1238.
- (18) Bauschlicher Jr., C. W. *J. Chem. Phys.* **1985**, *83*, 3129-3133.
- (19) Kusnetsov, A. M.; Nazumutdinov, R. R.; Shapnik, M. S. *Electrochim. Acta* **1989**, *34*, 1821-1828.
- (20) Ignaczak, A.; Gomes, J. A. N. F. *J. Electroanal. Chem.* **1997**, *420*, 209-218.
- (21) Seong, S.; Anderson, A. B. *J. Phys. Chem.* **1996**, *100*, 11744-11747.
- (22) Wright, K.; Hillier, I. H.; Vaughan, D. J.; Vincent, M. A. *Chem. Phys. Lett.* **1999**, *299*, 527-531.
- (23) Koper, M. T. M.; Santen, R. V. *J. Electroanal. Chem.* **1999**, *472*, 126-136.
- (24) Michaelides, A.; Hu, P. *J. Am. Chem. Soc.* **2001**, *123*, 4235.
- (25) Feibelman, P. J. *Science* **2002**, *295*, 99-102.
- (26) Michaelides, A.; Ranea, V. A.; de Andres, P. L.; King, D. A. *Phys. Rev. Lett.* **2003**, *90*, 216102.
- (27) Michaelides, A.; Alavi, A.; King, D. A. *Phys. Rev. B* **2004**, *69*, 113404.
- (28) Meng, S.; Wang, E. G.; Gao, S. *Phys. Rev. B* **2004**, *69*, 195404.
- (29) Michaelides, A.; Ranea, V. A.; Andres, P. L. d.; King, D. A. *Phys. Rev. B* **2004**, *69*, 075409.
- (30) Karlberg, G. S. *Phys. Rev. B* **2006**, *74*, 153414.
- (31) Wang, J. G.; Hammer, B. *J. Catal.* **2006**, *243*, 192-198.
- (32) Frisch *et al.*, M. J.; C.02 ed.; Gaussian Inc: Wallingford CT, 2004.
- (33) Becke, A. D. *J. Chem. Phys.* **1993**, *98*, 5648.
- (34) Lee, C.; Yang, W.; Parr, R. G. *Phys. Rev. B* **1988**, *37*, 785.
- (35) Cundari, T. R.; Stevens, W. J. *J. Chem. Phys.* **1993**, *98*, 5555.
- (36) Stevens, W.; Basch, H.; Krauss, J. *J. Chem. Phys.* **1984**, *81*, 6026.
- (37) Stevens, W. J.; Krauss, M.; Basch, H.; Jasien, P. G. *Can. J. Chem.* **1992**, *70*, 612.
- (38) Woon, D. E.; Dunning Jr., T. H. *J. Chem. Phys.* **1993**, *98*, 1358.
- (39) Wilson, A.; van Mourik, T.; Dunning Jr., T. H. *J. Mol. Struct.* **1997**, *388*, 339.
- (40) Peterson, K. A.; Woon, D. E.; Dunning Jr., T. H. *J. Chem. Phys.* **1994**, *100*, 7410.
- (41) Kendall, R. A.; Jr., T. H. D.; Harrison, R. J. *J. Chem. Phys.* **1992**, *96*, 6796.
- (42) Dunning Jr., T. H. *J. Chem. Phys.* **1989**, *90*, 1007.
- (43) Boys, S. F.; Bernardi, F. *Mol. Phys.* **1970**, *19*, 553.
- (44) Peng, C.; Schlegel, H. B. *Isr. J. Chem.* **1993**, *33*, 449-454.
- (45) Peng, C.; Ayala, P. Y.; Schlegel, H. B.; Frisch, M. J. *J. Comput. Chem.* **1996**, *17*, 49-56.
- (46) Gonzalez, C.; Schlegel, H. B. *J. Chem. Phys.* **1990**, *90*, 5523.

- (47) Gonzalez, C.; Schlegel, H. B. *J. Chem. Phys.* **1989**, *90*, 2154.
- (48) Wu, Z. J.; Han, B.; Dai, Z. W.; Jin, P. C. *Chem. Phys. Lett.* **2005**, *403*, 367-371.
- (49) Fritsch, D.; Koepernik, K.; Richter, M.; Eschrig, H. *J. Comp. Chem.* **2008**, *29*, 2210-2219.
- (50) Wang, G.-C.; Tao, S.-X.; Bu, X.-H. *J. Catal.* **2006**, *244*, 10-16.
- (51) Heras, J. M.; Papp, H.; Spiess, W. *Surf. Sci.* **1982**, *117*, 590.
- (52) Eyring, H. *J. Chem. Phys.* **2009**, *3*, 108-115.
- (53) Heras, J. M.; Albano, E. V. *Appl. Surf. Sci.* **1983**, *17*, 207.
- (54) Fischer, F.; Tropsch, H. *Ber. Dtsch. Chem. Ges.* **1926**, *59*, 830.
- (55) Zeinalipour-Yazdi, C. D.; Efstathiou, A. M. *J. Phys. Chem. C* **2008**, *112*, 19030-19039.
- (56) Evans, M. G.; Polanyi, N. P. *Trans. Faraday Soc.* **1938**, *34*, 11-29.
- (57) Brønsted, N. *Chem. Rev.* **1928**, *5*, 231-338.
- (58) Nørskov, J. K.; Bligaard, T.; Logadottir, A.; Bahn, S.; Hansen, L. B.; Bollinger, M.; Benggaard, H.; Hammer, B.; Sljivancanin, Z.; Mavrikakis, M.; Xu, Y.; Dahl, S.; Jacobsen, C. J. H. *J. Catal.* **2002**, *209*, 275-278.
- (59) Michaelides, A.; Liu, Z.-P.; Alavi, A.; King, D. A.; Hu, P. *J. Am. Chem. Soc.* **2002**, *125*, 3704-3705.
- (60) Logadottir, A.; Rod, T. H.; Nørskov, J. K.; Hammer, B.; Dahl, S.; Jacobsen, C. J. H. *J. Catal.* **2001**, *197*, 229-231.
- (61) Schumacher, N. M.; Boisen, A.; Dahl, S.; Gokhale, A. A.; Kandoi, S.; Grabow, L. C.; Dumesic, J. A.; Mavrikakis, M.; Chorkendorff, I. *J. Catal.* **2005**, *229*, 265-275.
- (62) Michaelides, A.; Alavi, A.; King, D. A. *J. Am. Chem. Soc.* **2003**, *125*, 2746-2755.